Published by IOP Publishing for Sissa Medialab

Received: *October 5, 2019*
Accepted: *November 29, 2019*
Published: *February 26, 2020*

21st International Workshop on Radiation Imaging Detectors
7–12 July 2019
Crete, Greece

2020 JINST 15 C02039

Operational experience and performance with the ATLAS Pixel detector at the Large Hadron Collider at CERN

Paolo Sabatini on behalf of the ATLAS collaboration

II. Physikalisches Institut, Georg-August-Universität Göttingen,
Friedrich-Hund-Platz 1, 37077 Göttingen, Germany

E-mail: paolo.sabatini@cern.ch

Abstract: During Run 2, the Large Hadron Collider (LHC) provided challenging running conditions for the ATLAS detector, and especially for the ATLAS Pixel Detector. This is the closest detector to the beam line, facing the highest event rate and radiation fluence. Despite the difficult environment, the Pixel detector has shown stable performance during data-taking, recording high quality data with high efficiency. However some lessons have been learned from the Run 2 operations, important for planning the coming Run 3. In particular, an understanding of the effects caused by radiation damage of the detector is crucial. Therefore dedicated measurements and simulations have been performed with the dataset collected in Run 2.

Keywords: Models and simulations; Particle tracking detectors (Solid-state detectors); Radiation damage to detector materials (solid state); Radiation damage to electronic components

https://doi.org/10.1088/1748-0221/15/02/C02039

Contents

2020 JINST 15 C02039

1 Introduction

The ATLAS Pixel Detector [1] is the innermost system of the ATLAS detector [2] and therefore subjected to the highest particle fluence. The detector configuration for Run 1 consisted of three concentric layers and three sets of ring-shaped endcaps on each side, at a distance of approximately 50 (B-Layer), 80 (Layer 1) and 122 mm (Layer 2) from the beam axis. After the end of Run 1, the Pixel Detector was upgraded with the installation of the Insertable B-Layer (IBL) [4, 5] at around 33 mm from the beam axis. The new detector layer was equipped with improved front-end chips and silicon sensors, more tolerant to radiation than the Run 1 Pixel Detector and also more performant in a "high-rate" environment; for which a reduced pixel size was chosen. With this upgrade, the detector is able to record three pixel hits for tracks up to $|\eta| < 2.5$.[1]

During Run 2, LHC performed far beyond the design expectations. The most challenging conditions have been reached in 2018, with a stable run at 2×10^{34} cm^{-2}s^{-1} of instantaneous luminosity (figure 1(a)) and an average number of interactions per bunch crossing (pile-up) of 36 (figure 1(b)), respectively 100% and 50% more than the design values. The study of the Pixel Detector response under the Run 2 conditions is crucial for the preparation for Run 3 (end 2020) when the current detector will face even more demanding conditions.

2 Detector performance during Run 2

Despite the unprecedented conditions, the Pixel detector has run smoothly over the whole Run 2, with an average efficiency of "high-quality" data recording above 99% [6], with only 4.7% of disabled modules at the end of the data-taking. The higher average number of tracks and hit rate did not affect the performance in terms of hit-on-track efficiency, which remained above 95% for every layer. The large particle fluence incident on the detector led to a decrease of the efficiency in the central part of the B-Layer, the innermost layer from the Run 1 installation. This inefficiency has been recovered by tuning the threshold differently for different η over the layer, as shown in

[1] The pseudo-rapidity η is defined as $\eta = -\ln(\theta/2)$, where θ is the polar angle from the beam axis.

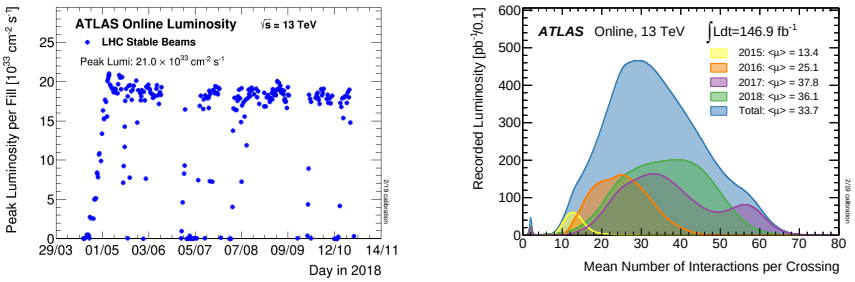

(a) (b)

Figure 1. LHC delivered instantaneous luminosity during 2018 data-taking (a). Pile-up distribution of the whole Run 2 (b) [3].

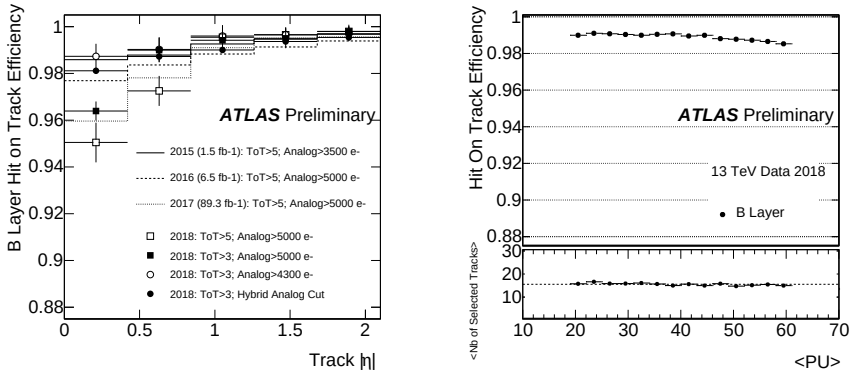

(a) (b)

Figure 2. Hit-on-track efficiency for the B-Layer for different signal threshold and Time-over-Threshold (ToT) settings in Run 2. Multiple configurations have been tested in 2018, and the *hybrid analog cut*, with different thresholds set over the detector, has been adopted (a). Hit-on-track efficiency for the B-Layer in 2018 over pile-up (b) [7].

figure 2(a). This configuration restored the layer performance, shown to be robust over pile-up (figure 2(b)).

Position and vertex resolution has benefited from the insertion of the additional layer, resulting in a very stable position resolution of 10 μm over time (figure 3(a)) and in an improvement in the secondary vertex identification. This feature plays a key role in physics analyses exploiting *b*-tagging algorithms, based on the reconstruction of secondary decay vertices, that got better in light- and *c*-jets background rejection with respect to Run 1 (figure 3(b)).

3 Experience from the data acquisition system

The high data quality and efficiency of the detector attests to the robustness of the data acquisition system during Run 2. However, some lessons have been learned from the data-taking and some actions are required to get the detector ready for Run 3.

An important cause of unrecoverable modules in Run 2 is the failure of the laser array (VCSEL) that transmits data via optical fibres from the detector to off-detector electronics. These VCSELs are mounted on the *opto-board*; their failure breaks the communication path from the modules to

2020 JINST 15 C02039

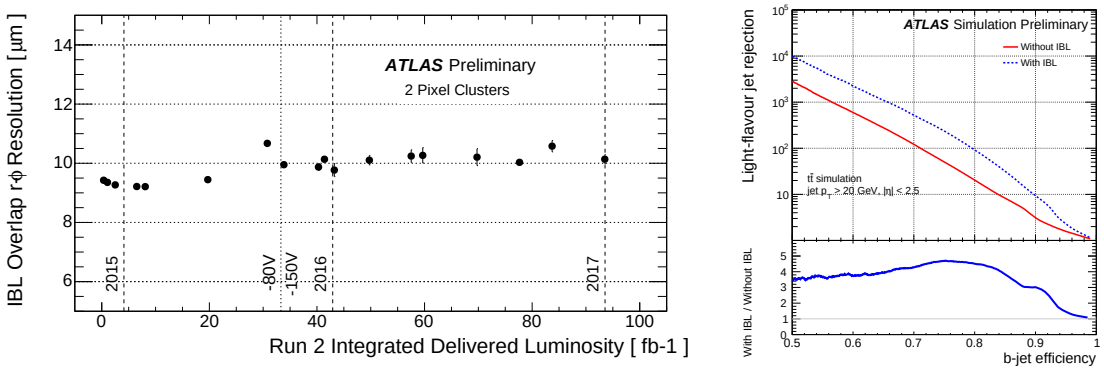

(a) (b)

Figure 3. Position resolution for the IBL versus integrated luminosity (a) [7]. Improvement in *b*-tagging performance with the insertion of the IBL in Run 2 (b) [8].

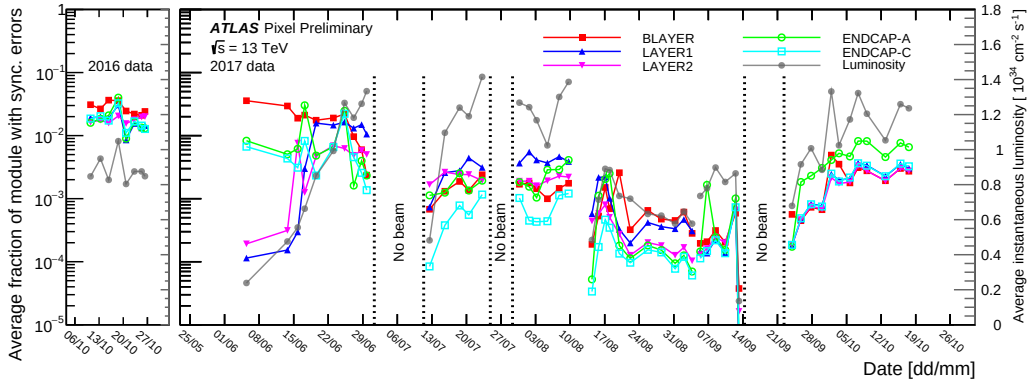

Figure 4. Fraction of modules with desynchronisation errors per event over time [7].

the off-detector. The only way to recover such a failure is the replacement of the opto-board where the problematic VCSEL is located. 34 boards have been replaced during the 2017–2018 Year-End-Technical Stop (YETS) but 21 new failures were already identified during 2018 data-taking.

Recoverable, but frequent, errors from the readout chain are the *desynchronisation errors*. These are due to the convolution of two factors: the high trigger rate (that depends on the instantaneous luminosity) and the large event size (that depends on the hit occupancy). When both factors are present, a temporary saturation of the link bandwidth may occur, causing overflows in the FE or in the off-detector buffers, leading to the creation of broken events associated to the wrong bunch-crossing or trigger. As shown in figure 4, the incidence of this type of error depends on the instantaneous luminosity. A mitigation of the impact of such errors is obtained by periodically resetting (every 5 s) the front-end chip and off-detector electronics and reconfiguring the front-ends. This procedure has been introduced in 2017, leading to a drastic decrease of the fraction of modules affected by desynchronisation errors (figure 4).

2020 JINST 15 C02039

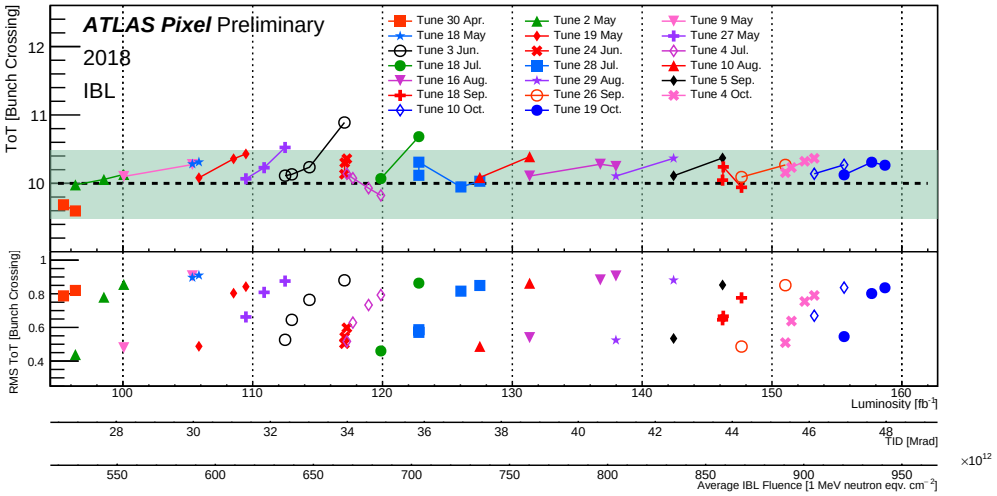

Figure 5. Time-over-Threshold (ToT) of the signal over integrated luminosity [7].

4 Measurements of the radiation damage

The validation and improvement of models for the radiation damage of the detector is critical for the operations in Run 3. Run 2 data are therefore used to study the impact on the detector performance and predict the conditions for the future data-taking.

A first observed effect is the reduction of the hit occupancy in the detector (and of bandwidth occupancy as a consequence). This is strictly connected to a decrease in the efficiency due to a lower charge collection. Dedicated tuning of the signal threshold has been performed on B-Layer (figure 2(a)) and IBL, to restore high efficiency.

An effect of radiation on the front-end chips, installed in the IBL, is the drift of the leakage current of the on-chip charge amplifier circuit that shapes the input electrical signal from the sensor. This results in a drift of the Time-over-Threshold (ToT) of the measured charge signal over time, as shown in figure 5. A plan of periodic recalibration has been introduced in 2018 to recover the correct ToT and charge information. For that year, IBL has been tuned to provide a ToT equal to 10 bunch crossing (BC) for 16 ke of injected charge (expected MIP charge deposition), with a threshold on the signal of 2 ke. The importance of the recalibration campaign in 2018 is clear from figure 5, since the ToT is restored to the target value and the ToT distribution gets shrunk (reduction of ToT distribution RMS) after every tuning.

The most important direct effect of damage in the structure of the sensor bulk is definitely the reduction of charge collection. This impacts the value of the measured ionised charge in the sensor, and therefore the measured dE/dx of the traversing particle. In fact, a clear trend in dE/dx has been observed over time in the two innermost layers, the IBL (figure 6(a)) and B-Layer (figure 6(b)). The decrease of the charge collection efficiency is a crucial parameter to optimise the running condition for Run 3, and to understand the future response of the detector. Therefore, a reliable modelling of the damage and its impact on the detector measurements is needed. ATLAS has developed a dedicated Radiation Damage simulation [9], whose prediction on charge collection results in good agreement with measured data (figure 7).

2020 JINST 15 C02039

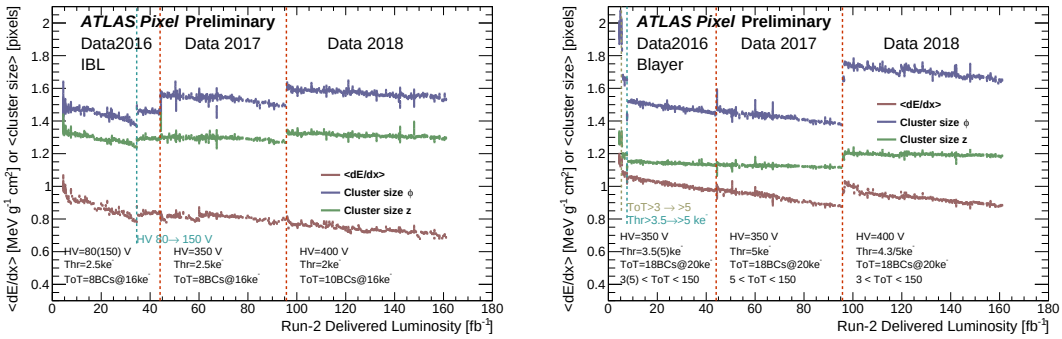

(a) (b)

Figure 6. Measurement of the dE/dx over integrated luminosity in the IBL (a) and B-Layer (b) [7].

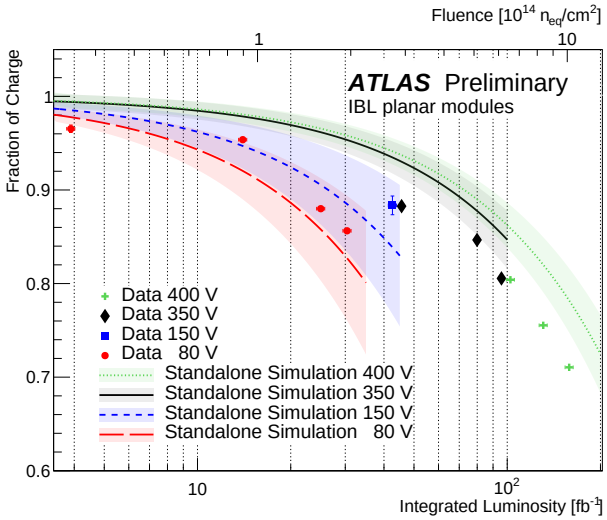

Figure 7. Comparison of the simulation of the fraction of collected charge over integrated luminosity with observed data. Because of the different high voltage applied to the module during Run 2 (80 and 150 V in 2016, 350 V in 2017 and 400 V in in 2018), a dedicated simulation is performed for each setting and compared with the corresponding period data points. The prediction is performed with the ATLAS Radiation Damage simulation [7].

A parameter affecting the charge collection is the high voltage bias applied to the module. However, damage in the bulk causes an increase of the voltage needed for a full depletion of the sensor depth, the depletion voltage. Studies of the evolution of the depletion voltage are needed to foresee the operational condition for Run 3. Independent measurements from different environments result in a compatible trend of the depletion voltage with the absorbed radiation (figure 8(a)). The difference in radiation fluence over $|\eta|$ of the detector has been used to measure the relative change of the depletion voltage (figure 8(b)) and to compare it with the radiation fluence predictions (figure 8(c)). The observed change in the depletion voltage is compatible with the same measurement performed on the leakage current (figure 8(b), bottom panel) and consistent with the tuned fluence prediction.

2020 JINST 15 C02039

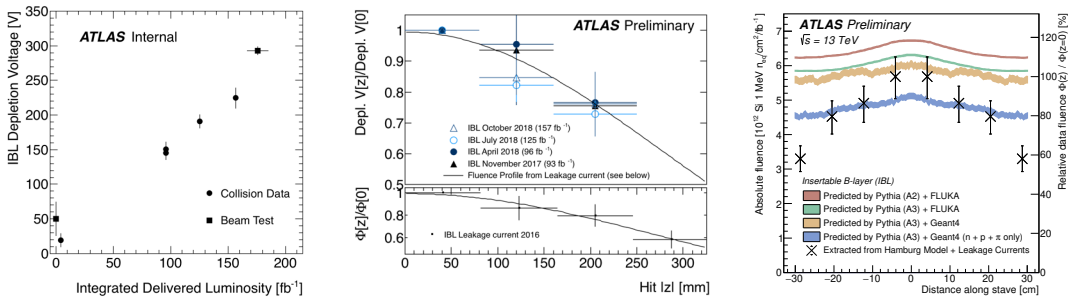

(a) (b) (c)

Figure 8. Comparison of the depletion voltage evolution observed in collision and dedicated beam test datasets (a). Evolution of the depletion voltage with $|\eta|$ for IBL (b). Prediction of radiation fluence against $|\eta|$ for IBL (c) [7].

5 Summary

During Run 2, the LHC provided unprecedented conditions in terms of pile-up and instantaneous luminosity. Despite the challenging environment, the ATLAS Pixel Detector had a very smooth operation with high data quality and efficiency.

The experience from Run 2 is crucial to plan for Run 3 operations, and to quantify and test solutions for the upcoming challenges. The VCSELs failures in the Pixel Run 1 opto-boards have been quite an important cause of disabled modules during the run and a replacement plan is under discussion for Run 3. An automated procedure to mitigate desynchronisation errors has been successfully implemented in Run 2 and further improvements are expected in Run 3 exploiting the readout system capabilities.

The main challenge is to quantify and predict the detector radiation damage, whose effects are already visible in Run 2 data. A dedicated simulation has been deployed to model the detector response under such conditions. The predictions have shown good agreement with results from dedicated measurements on the Run 2 dataset, and have been used to extrapolate for Run 3 conditions.

References

[1] G. Aad et al., *ATLAS pixel detector electronics and sensors*, 2008 *JINST* **3** P07007.

[2] ATLAS collaboration, *The ATLAS experiment at the CERN Large Hadron Collider* 2008 *JINST* **3** S08003.

[3] ATLAS collaboration, *Public luminosity plots for run 2*, https://twiki.cern.ch/twiki/bin/view/AtlasPublic/LuminosityPublicResultsRun2.

[4] ATLAS collaboration, *ATLAS insertable B-layer technical design report*, CERN-LHCC-2010-013 (2010) [ATLAS-TDR-19].

[5] ATLAS IBL collaboration, *Production and integration of the ATLAS insertable B-layer*, 2018 *JINST* **13** T05008.

[6] ATLAS collaboration, *Public run statistics plots*, https://twiki.cern.ch/twiki/bin/view/AtlasPublic/RunStatsPublicResults2010.

2020 JINST 15 C02039

[7] ATLAS collaboration, *Public pixel tracker plots*, https://twiki.cern.ch/twiki/bin/view/AtlasPublic/PixelPublicResults.

[8] ATLAS collaboration, *Public flavour tagging plots*, https://twiki.cern.ch/twiki/bin/view/AtlasPublic/PixelPublicResults.

[9] ATLAS collaboration, *Modelling radiation damage to pixel sensors in the ATLAS detector*, 2019 *JINST* **14** P06012.

2020 JINST 15 C02039